IEEE Access
Multidisciplinary | Rapid Review | Open Access Journal

Received September 6, 2020, accepted September 9, 2020, date of publication September 14, 2020,
date of current version September 24, 2020.

Digital Object Identifier 10.1109/ACCESS.2020.3023717

An Improved Nonlinear Predictive Control Strategy Enhanced by Fractional Order Extremum Seeking Control of the Antilock Braking System of a Vehicle

REN HE AND LEI YUAN
School of Automobile and Traffic Engineering, Jiangsu University, Zhenjiang 212013, China
Corresponding author: Lei Yuan (18796016197@163.com)

This work was supported in part by the National Natural Science Foundation of China under Grant 51875258, and in part by the Key Research and Development Plans of Zhenjiang under Grant 2018022.

ABSTRACT Extremum seeking control can search the optimal slip rate of the antilock braking system of a vehicle through a high-frequency sinusoidal excitation signal. However, because of the bandwidth limitation of the braking actuator, the search speed of the optimal slip rate decreases and the stability of the extremum seeking control system becomes worse. To search and control the optimal slip rate, an improved nonlinear predictive control strategy enhanced by fractional order extremum seeking control is proposed for the vehicle antilock braking system. First, the nonlinear dynamic model of the braking system is established. Then, nonlinear prediction control is designed with the prediction of the slip rate response based on the nonlinear model to achieve slip rate control. Using fractional order calculus, a fractional extremum seeking controller is proposed to search for the optimal slip rate. Nonlinear predictive control integrated with fractional extremum seeking control is proposed to achieve the function of vehicle antilock braking. Finally, the effectiveness of the proposed method is verified by simulating the vehicle antilock braking system under different road conditions. The result shows that by considering the actuator available bandwidth, the proposed fractional order extremum seeking control can improve the search speed of the optimal slip rate compared with traditional integer order extremum seeking control. The proposed integrated controller achieves wheel slip rate optimal control regardless of the road conditions.

INDEX TERMS Extremum seeking control, fractional order, ABS, nonlinear predictive control, slip rate.

I. INTRODUCTION

With the development of the automobile industry, automobile safety requirements have risen, especially the braking performance at high speeds [1]–[3]. The antilock braking system (ABS) is an active safety device that is used to control and adjust the braking torque to prevent the wheels from locking during braking, so that the vehicle makes maximum use of the ground adhesion to slow down and stop [4], [5]. Therefore, the ABS plays a vital role in vehicle driving safety. With the development of new energy vehicles and autonomous vehicles, the technology of the brake-by-wire system has been greatly developed [6], [7]. Using the brake-by-wire system to control the slip rate improves not only the ABS performance of traditional vehicles but also the ABS performance of new energy vehicles and autonomous vehicles.

Although the ABS has been widely used in automobiles, designing an ABS controller with better performance has remained a challenge until now [8]. The difficulty in designing the ABS controller arises from two main reasons. First, the ABS is a strongly nonlinear system. Second, changes in the road conditions cause uncertainty in control objectives. For the first problem, numerous nonlinear controllers were designed, such as sliding mode control (SMC) [9], PID control [10], model predictive control (MPC) [2], nonlinear optimal control [11], [12], fuzzy logic control [13], neural network control [14], [15], iterative learning control [16], and other intelligent control methods [17]. The SMC method was widely used in control engineering because of its potential for handling the nonlinearity and to achieve the inherent

The associate editor coordinating the review of this manuscript and approving it for publication was Choon Ki Ahn.

robustness. Reference [18] used the memory and genetic properties of a fractional order calculation to design a fractional order SMC for antilock control. Reference [10] suggested that the combination of a fractional order sliding mode controller (FOSMC) and fuzzy logic control (FLC) further improved the robust performance of the ABS. However, the application of sliding mode control is restricted by its chattering effect. References [11] and [12] proposed an ABS nonlinear predictive control method and applied it to predicting the nonlinear response of a continuous nonlinear vehicle dynamics model. Through integral feedback technology and radial basis neural network technology, a better ABS performance is obtained compared to that of SMC. Reference [19] considered asymmetric slip rate constraints to track the optimal slip rate. The above control strategies all adopted a fixed slip rate regardless of the changing road conditions. However, the actual tire longitudinal characteristics indicate that the corresponding optimal slip rate varies under different road conditions.

To solve the second problem, much research has focused on automatically identifying road surface friction coefficients online and automatically adjusting the target slip rate according to the identified road conditions [20]–[22]. Reference [20] proposed a road adhesion coefficient recognition method based on IMM Kalman filtering. Reference [21] proposed a method for estimating the tire-road friction coefficient in real time that can independently estimate the friction coefficient of the front and rear wheels. However, automatic identification requires additional sensors to be installed on the vehicle, which increases the hardware costs. The algorithm is complex, and the poor real-time performance under emergency braking conditions also limits the application. Extremum seeking control (ESC) can adaptively converge and stabilize the optimal slip rate without the road surface friction coefficient recognition, which is an effective way to solve the second problem [23], [24]. Great progress has been made in parameter design, stability analysis, structural design of control systems, and performance improvement of the ESC algorithm. In [25], fractional-order calculus was used to improve the convergence speed of ESC, and the stability of fractional order extremum seeking control (FOESC) was proved. Scholars have studied the application of ESC in the ABS system. Reference [26] proposed an improved sliding mode extremum seeking control method that addressed the problem of time delay in the ABS and solved the problem of excessive oscillation of the system. Reference [27] treated the problem of extremum seeking control as an optimization problem with dynamic system constraints. An ESC control scheme based on numerical optimization was proposed and applied to the ABS. In [28], an ESC was successfully designed, and the steering law was adopted to modify the control law to compensate the lateral stability of the vehicle during cornering. However, the ESC algorithm scarcely considers the limitation of the brake actuator bandwidth. Gunter Stein proposed the concept of available bandwidth and the limitation principle through frequency domain analysis [29]. He emphasized the importance of actuator bandwidth to control system design.

Therefore, the available bandwidth is very important and must be considered in the design process of the ABS controller. Limited by the available bandwidth of the actuator, the convergence speed of ESC will be reduced. The fractional algorithm can improve the stability and response speed of ESC. To our knowledge, the application of FOESC to the ABS is completely unexplored. This article studies the ABS control based on an integrated control combining nonlinear predictive control (NPC) and FOESC. FOESC is proposed to search the optimal slip rate. NPC is developed to predict the slip rate response from the nonlinear vehicle model and control the searched slip rate. Compared with the traditional integer order extremum seeking control (IOESC), the FOESC algorithm improves the search speed of the optimal slip rate with the available bandwidth of the braking actuator.

The remainder of this article is arranged as follows. Section II introduces the definition of fractional calculus. In Section III, the dynamic model is established. Section IV presents the results of the ABS controller design. Section V illustrates the superiority and effectiveness of the proposed control method through simulation. Section VI draws the conclusion of this article.

II. DEFINITION OF FRACTIONAL CALCULUS

Fractional calculus has a 300-hundred year history, but it initially focused primarily on theoretical research. In recent years, the application of fractional calculus theory has begun in many fields, such as the new theory of fractional order control in the field of automation.

There have been many definitions of fractional calculus during its development, such as the Cauchy integral formula directly extended by integral order, the Grunwald-Letnikov fractional order calculus definition, the Riemann-Liouville fractional order definition of integration and the definition of Caputo fractional calculus.

A. DEFINITION OF THE GRUNWALD-LETNIKOV FRACTIONAL CALCULUS

The Grunwald-Letnikov integral formula is directly extended from the simple integer order integration.

$$ {}_aD_t^{\alpha} f(t) = \lim_{h\to 0} \frac{1}{h^{\alpha}} \sum_{j=0}^{[(t-\alpha)/h]} (-1)^j \binom{\alpha}{j} f(t-jh) \quad (1) $$

where $w_j^{\alpha} = (-1)^j \binom{\alpha}{j}$ is the polynomial coefficient of $(1-z)^{\alpha}$.

The coefficient is obtained directly from the following recursive equations:

$$ w_0^{\alpha} = 1, w_j^{(\alpha)} = \left(1 - \frac{\alpha+1}{j}\right) w_{j-1}^{(\alpha)}, \quad j = 1, 2, \cdots \quad (2) $$

According to this definition, the algorithm for fractional differential calculation can be derived as

$$ {}_aD_t^{\alpha} f(t) = \lim_{h\to 0} \frac{1}{h^{\alpha}} \sum_{j=0}^{[(t-a)/h]} (-1)^j \binom{\alpha}{j} f(t-jh) \quad (3) $$

Assuming that the step size h is sufficiently small, the above equation can be used to directly find the approximate value of the function's numerical differentiation. The accuracy of this formula is denoted $o(h)$.

B. DEFINITION OF THE RIEMANN-LIOUVILLE FRACTIONAL CALCULUS

The Riemann-Liouville fractional order integral is defined as

$$ {}_aD_t^{-\alpha} f(t) = \frac{1}{\Gamma(\alpha)} \int_a^t (t-\tau)^{\alpha-1} f(\tau)\, d\tau \quad (4) $$

Fractional differentiation is also defined by such integration. Assuming the fractional order $n-1 < \beta \le n$, the fractional order differential is defined as

$$ \begin{aligned} {}_aD_t^{\beta} f(t) &= \frac{d^n}{dt^n}\left[{}_aD_t^{-(n-\beta)} f(t)\right] \\ &= \frac{1}{\Gamma(n-\beta)} \frac{d^n}{dt^n}\left[\int_a^t \frac{f(\tau)}{(t-\tau)^{\beta-n+1}} d\tau\right] \end{aligned} \quad (5) $$

C. DEFINITION OF THE CAPUTO FRACTIONAL CALCULUS

The Caputo fractional differential is defined as

$$ {}_0D_t^{\alpha} y(t) = \frac{1}{\Gamma(1-\gamma)} \int_0^t \frac{y^{(m+1)}(\tau)}{(t-\tau)^{\gamma}} d\tau \quad (6) $$

where $\alpha = m+\gamma$; m is an integer; and $0 < \beta \le 1$. Similarly, Caputo fractional integration is defined as

$$ {}_0D_t^{\gamma} = \frac{1}{\Gamma(-\gamma)} \int_0^t \frac{y(\tau)}{(t-\tau)^{1+\gamma}} d\tau, \gamma < 0 \quad (7) $$

III. DYNAMICS MODEL

A. VEHICLE DYNAMICS MODEL

The 1/4 vehicle model is applied, as shown in Fig. 1. The dynamic behavior of the model is expressed as

$$ \dot{v} = \frac{-F_x}{m_t} \quad (8) $$

$$ \dot{w} = \frac{1}{I_t}(RF_x - T_b) \quad (9) $$

where R is the wheel radius; I_t is the wheel inertia; v is the vehicle speed; w is the wheel angular velocity; T_b is the braking torque; F_x is the tire longitudinal force; and m_t is the quarter vehicle total mass.

The tire longitudinal force F_x depends on the vertical load of the tire. The vertical load consists of two parts: the static load due to the vehicle's mass distribution, and the tire dynamic load generated during braking. Therefore, the vertical load of the rear tire of the 1/4 vehicle model is

$$ F_z = m_t g - \frac{m_{vs} h_{cg}}{2l} a = m_t g - F_L \quad (10) $$

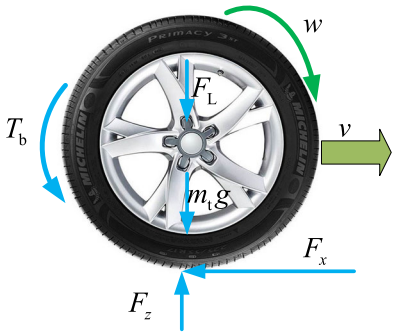

FIGURE 1. Single wheel dynamics model.

where l is the wheelbase; $h_{cg}$is the height of the mass center; and F_L is the dynamic load.

The slip rate of the tire is expressed as

$$ \lambda = \frac{v - Rw}{v} \quad (11) $$

Differentiating the slip rate by time, we obtain

$$ \dot{\lambda} = \frac{\dot{v}(1-\lambda) - R\dot{w}}{v} \quad (12) $$

Substituting (8) and (9) into (12) gives

$$ \dot{\lambda} = -\frac{1}{v}\left[\frac{F_x}{m_t}(1-\lambda) + \frac{R^2 F_x}{I_t}\right] + \left(\frac{R}{vI_t}\right) T_b \quad (13) $$

Equations (8) and (13) constitute the state-space equations for the vehicle braking system. The vehicle speed v and the slip rate λ are state vectors, and the braking torque T_b is the control vector.

B. TIRE MODEL

The tire longitudinal force F_x is a function of the tire longitudinal slip rate. When the longitudinal slip rate is small, the longitudinal force is linearly related to the slip rate. As the slip rate increases, the tire longitudinal force F_x reaches a maximum value. When the slip rate is greater than the optimal slip rate value, the tire longitudinal force decreases with increasing slip rate.

We use the Dugoff tire model. The tire longitudinal force is expressed as

$$ F_x = \frac{C_i \lambda}{1-\lambda} f(\sigma) \quad (14) $$

where

$$ f(\sigma) = \begin{cases} \sigma(2-\sigma)\, i & \text{if } \sigma < 1 \\ 1 & \text{if } \sigma > 1 \end{cases}, $$

$$ \sigma = \frac{uF_z\left(1-\varepsilon_r v\sqrt{\lambda^2+\tan^2\alpha}\,(1-\alpha)\right)}{2\sqrt{C_i^2\lambda^2 + C_\alpha^2 \tan^2\alpha}}, $$

and where C_α is the cornering stiffness of the tire; μ is the road friction coefficient; ε_r is the factor of road adhesion reduction; and C_i is the tire longitudinal stiffness.

C. REFERENCE SLIP MODEL

To avoid a large slip rate tracking error, a reference model of tire slip transient response is established, and the reference model of tire slip is expressed as

$$\lambda_{\mathrm{d}}(s) = \frac{\lambda_{\mathrm{opt}}}{s}\frac{\mathrm{a}}{s+\mathrm{a}} \tag{15}$$

where λ_{opt} is the target slip; and a is the time constant [29]. The inverse Laplace transform is performed on both sides of (8), and then the first order zero initial condition differential equation is obtained:

$$\lambda_{\mathrm{d}}(t) = \lambda_{\mathrm{opt}} - \lambda_{\mathrm{opt}} e^{-at} \tag{16}$$

Equation (16) describes a wheel slip reference model in the time domain. Based on this model, a nonlinear controller is designed to control the optimal slip rate.

IV. CONTROL METHOD OF ABS

A. Design of NPC

The NPC is used to realize the ABS function. Equations (8) and (13) are used to construct the dynamic state equation of the ABS. The slip rate is used as the system output, and the state space is expressed as follows:

$$\dot{x}_1 = \frac{F_x}{m_t} \tag{17}$$

$$\dot{x}_2 = \frac{F_x}{x_1}\left(\frac{1-x_2}{m_t} + \frac{R^2}{I_t}\right) + \frac{R}{I_t x_1} T_b \tag{18}$$

To improve the robustness of the controller, the slip rate and slip rate integral are selected as the control targets of the ABS. The new state variable x_3 is defined as follows:

$$\dot{x}_3 = x_2 \tag{19}$$

The purpose of the control system is to control the tire slip x_2 and its integral x_3 to converge to the optimal slip rate.

The idea behind the NPC is that a Taylor series expansion can be used to predict the state vector $x(t+h)$ at the next time. The concept of the prediction step h is similar to the concept of the prediction time domain in model predictive control. The control T_{b} is calculated according to the principle of minimizing the tracking error.

The state variables x_2 and x_3 are selected as the output of the system, and a performance function is constructed to optimize the tracking error at the next moment:

$$J = \frac{1}{2} w_2 \left[x_2(t+h) - x_{2\mathrm{d}}(t+h)\right]^2 + \frac{1}{2} w_3 \left[x_3(t+h) - x_{3\mathrm{d}}(t+h)\right]^2 \tag{20}$$

which can be simplified as follows:

$$J = \frac{1}{2}\sum_{\mathrm{n}=2}^{3} w_n \left[x_n(t+h) - x_{n\mathrm{d}}(t+h)\right]^2 \tag{21}$$

where w_2 and w_3 are the weight coefficients of the tire slip rate and its integral, respectively.

The k order Taylor series of the state vector at time t is approximated as follows:

$$x_n(t+h) = x_n(t) + h\dot{x}_n(t) + \frac{h^2}{2!}\ddot{x}_n + \cdots + \frac{h^{k_n}}{k_n!} x_n^{(k_n)}(t) \quad n = 2, 3 \tag{22}$$

The control order is one of the controller design parameters and must be a compromise between performance and input energy consumption. A sufficient condition for a Taylor series prediction is that the control order is not lower than the order of the prediction vector. Therefore, x_2 is expanded as a first-order Taylor series, and x_3 is expanded as a second-order Taylor series:

$$x_2(t+h) = x_2(t) + h\dot{x}_2(t) \tag{23}$$

$$x_{3\mathrm{d}}(t+h) = x_{3\mathrm{d}}(t) + h\dot{x}_{3\mathrm{d}}(t) + \frac{h^2}{2!}\ddot{x}_{3\mathrm{d}} \tag{24}$$

Similarly, a Taylor series expansion is performed on the state vector of the reference slip rate:

$$x_{2\mathrm{d}}(t+h) = x_{2\mathrm{d}}(t) + h\dot{x}_{2\mathrm{d}}(t) \tag{25}$$

$$x_{3\mathrm{d}}(t+h) = x_{3\mathrm{d}}(t) + h\dot{x}_{3\mathrm{d}}(t) + \frac{h^2}{2!}\ddot{x}_{3\mathrm{d}} \tag{26}$$

Therefore, by introducing (23)-(26) into (21), the performance function is obtained with the control input as a variable. According to the optimal theory, the necessary condition for the optimization of the performance function is

$$\frac{\partial J}{\partial T_b} = 0 \tag{27}$$

which leads to

$$T_b(t) = -\frac{x_1 I_t}{Rh}\frac{1}{1+0.25\beta h^2} \cdot \begin{bmatrix} \left(1+0.5\beta h^2\right) e_2 + (0.5\beta h)\, e_3 \\ +h\left(1+0.25\beta h^2\right)\left(-\frac{F_x}{v}\left(\frac{1-\lambda}{m_t} + \frac{R^2}{I_t}\right) - \dot{x}_{2\mathrm{d}}\right) \end{bmatrix} \tag{28}$$

where e_2 and e_3 are the tracking errors of the output: $e_2 = x_2(t) - x_{2\mathrm{d}}(t)$; $e_3 = x_3(t) - x_{3\mathrm{d}}(t)$; $\beta = \frac{w_3}{w_2} \geq 0$.

B. DESIGN OF FOESC

The traditional IOESC based on a disturbance signal is combined with NPC to realize the ABS function. The schematic is shown in Fig. 2. The purpose of NPC is to track the tire slip rate according to the IOESC requirements. The IOESC uses the braking deceleration as the objective function and the sine function as the disturbance to obtain the direction of the convergence gradient.

According to the basic principles of the above IOESC, the mathematical model of the IOESC can be expressed as follows:

$$z = f\left(\tilde{\lambda} + d\sin(\omega t)\right)$$

$$\dot{\tilde{\lambda}} = -k\xi$$

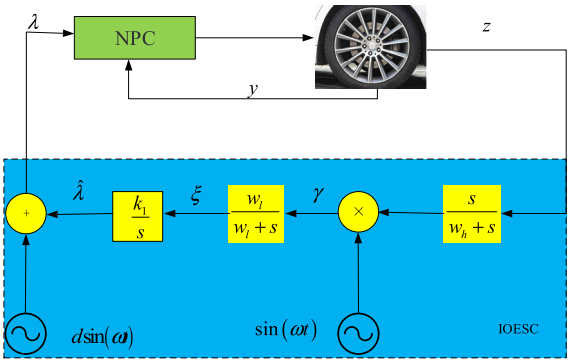

FIGURE 2. Schematic of IOESC.

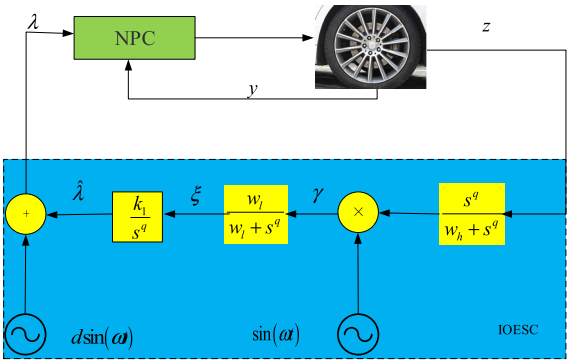

FIGURE 3. Schematic of FOESC.

$$\begin{aligned}\xi &= k * L^{-1}\{G_{LPF}(s)\}\\ \gamma &= \left[z * L^{-1}\{G_{HPF}(s)\}\right]\sin(\omega t)\end{aligned} \tag{29}$$

where the sinusoidal excitation signal is $d\sin(\omega t)$; k_1 is the IOESC gain factor; $G_{HPF}(s)$ is the transfer function of a first-order high-pass filter; $G_{LPF}(s)$ is the transfer function of the first-order low-pass filter; z is the braking deceleration; y in Fig. 2 is the actual tire slip during braking; $\hat{\lambda}$ is the slip obtained from the ESC search; λ is the target slip that is actually applied to the nonlinear control system; and γ is the gradient signal obtained by multiplying the braking deceleration with a sinusoidal excitation signal after high-pass filtering.

The average linearization model of the slip rate $\hat{\lambda}$ obtained from the ESC search and the optimal slip rate λ^* is

$$\frac{\tilde{\lambda}}{\lambda^*} = \frac{1}{1+L(s)} \tag{30}$$

where $\tilde{\lambda} = \hat{\lambda} - \lambda^*$, and

$$\begin{aligned}L(s) &= \frac{kd^2}{2s}\left(e^{j\phi}\frac{s+j\omega}{s+j\omega+\omega_h} + e^{-j\phi}\frac{s-j\omega}{s-j\omega+\omega_h}\right)\\ L(s) &= \frac{kd^2}{2s}\left(e^{j\phi}\frac{s+j\omega}{s+j\omega+\omega_h} + e^{-j\phi}\frac{s-j\omega}{s-j\omega+\omega_h}\right)\end{aligned} \tag{31}$$

Equation (31) is used for the stability analysis of the IOESC average model. If the phase delay of the disturbance signal is set to 0, the model can be simplified to

$$\frac{\lambda(s)}{\lambda^*(s)} = \frac{s\left(s^2+2\omega_h s+\omega_h^2+\omega^2\right)}{s^3+\left(2\omega_h+kd^2\right)s^2+\left(\omega_h^2+\omega^2+kd^2\omega_h\right)s+kd^2\omega^2} \tag{32}$$

Equation (32) shows that the system is in a stable state when $k_1 > 0$.

However, the closed-loop transfer function (32) has a pair of poles near the imaginary axis, which cause a slight damping effect and the slow convergence rate of the ESC system. If the closed-loop transfer function integer order of the average model of ESC is replaced with a fractional order, no pole is near the stable boundary of the fractional order closed-loop transfer function. Therefore, the system has a very fast convergence speed and a more robust performance.

We propose to use FOESC to search for the optimal slip rate of the ABS. The integer order integral $\frac{1}{s}$ is replaced by the fractional order integral $\frac{1}{s^q}$, and high-pass filters are replaced by fractional-order filters $\frac{s^q}{\omega_h+s^q}$, where q is the fractional value, as shown in Fig. 3.

The $L(s)$ in FOESC is expressed as

$$L(s) = \frac{\gamma d^2}{s^q}\frac{s^{2q}+\omega_h s^q+\omega^2}{s^{2q}+2\omega_h s^q+\omega^2+\omega_h^2} \tag{33}$$

By defining $\rho = s^q$, the average linearized models of λ and λ^* for FOESC can be described as

$$\frac{\tilde{\lambda}(\rho)}{\lambda^*(\rho)} = \frac{\rho\left(\rho^2+2\omega_h\rho+\omega_h^2+\omega^2\right)}{\rho^3+\left(2\omega_h+kd^2\right)\rho^2+\left(\omega_h^2+\omega^2+kd^2\omega_h\right)\rho+kd^2\omega^2} \tag{34}$$

The GL formula calculates the fractional differential of a given signal more accurately, but this type of algorithm has great limitations in the study of control systems. Such an algorithm needs to calculate the sampled value of the signal in advance. The value of the function is unknown in the simulation of the control system, so the Oustaloup filter algorithm is used to approximate the fractional differential value [30]. Assuming that the selected fitting frequency band is (w_b, w_t), the transfer function model of the continuous filter is be constructed as

$$G_f(s) = K\prod_{k=-N}^{N}\frac{s+w_k'}{s+w_k} \tag{35}$$

The zero, pole and gain of the filter are directly obtained from the following formulas:

$$\begin{aligned}w_k' &= w_b\left(\frac{w_t}{w_b}\right)^{\frac{K+N+\frac{1}{2}(1-\gamma)}{2N+1}},\\ w_k &= \left(\frac{w_t}{w_b}\right)^{\frac{K+N+\frac{1}{2}(1+\gamma)}{2N+1}}, \quad K = w_t^{\gamma}.\end{aligned}$$

where γ is the fractional order; $2N+1$ is the order of the filter; and w_b and w_t are the lower and upper limits of the fitting frequency, respectively. Generally, the fractional differential operator is fitted well in this region, while the

TABLE 1. Simulation parameters.

parameter	Value	parameter	Value
v/ m·s^{-1}	30	ε_r/ s·m^{-1}	0.015
R/ m	0.326	a	20
m_{vs}/ kg	415	ω_l / ms	0.6
m_w/ kg	40	ω_h /ms	0.8
h_{cg} /m	0.5	I_t /kg·m^2	1.7
C_i/ N·slip^{-1}	30000	h	0.01
C_α/ N • rad^{-1}	50000	β	1
k_1	9	k_2	30
d	0.001	ω	5
q	0.7	τ_b /ms	54.3
ω_b	0.001	w_t	10000

other regions are very different from the differential operator. The presented algorithm avoids the limitations of $w_b w_h = 1$ with two arbitrary frequency.

V. SIMULATION RESULTS

To verify the effectiveness of the integrated control of NPC enhanced by FOESC, the ABS simulation and comparison analysis of NPC enhanced by FOESC and IOESC, which are hereafter referred to as FOESC and IOESC, were performed on a single road and a changing road. Based on whether the bandwidth of the actuator is considered, the ABS simulation performance of the two control methods is studied. The expression for the braking torque without considering the actuator bandwidth is

$$T_b = T_{\text{ideal}} \tag{36}$$

The brake torque expression considering the actuator bandwidth is [31], [32]

$$T_b = \frac{T_{\text{ideal}}}{1 + \tau_b} \tag{37}$$

The simulation parameters are shown in Table 1 [11], [29]. Different road adhesion coefficients result in different tire mechanical properties. First, the relationship between the slip rate and braking torque is simulated for a high adhesion road, medium adhesion road, and low adhesion road. The adhesion coefficients u of the high, medium, and low adhesion roads were selected as 0.8, 0.5, and 0.3, respectively. Fig. 4 shows that the optimal slip rates on high, medium, and low adhesion pavements are 0.11, 0.088, and 0.068, respectively. In the following simulations, the tire characteristics shown in Fig. 4 are all used for simulation analysis.

Fig. 5 (a) and Fig. 5 (b) compare the braking torque of FOESC and IOESC with the ideal actuator and the available bandwidth actuator, respectively, on the high adhesion road. When using the ideal controller, FOESC has a 1709 N·m peak torque in the early stage of braking. This behavior allows the tire to reach the target slip rate faster. The IOESC braking torque peak is 555 N·m at the initial stage of braking. The slip rate reaches the optimal slip rate near 0.11 without overshoot. When using the available bandwidth actuator, the IOESC

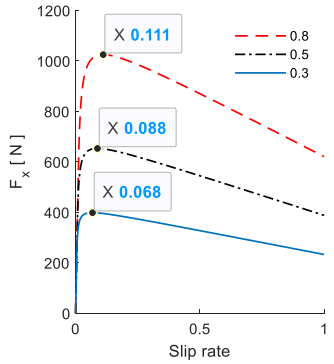

FIGURE 4. Wheel slip rate versus the longitudinal tire force on the different roads.

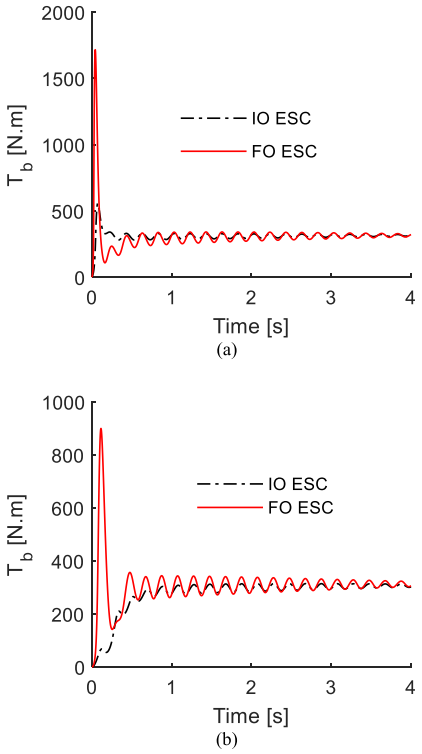

FIGURE 5. Braking torque curve on the high adhesion road. Comparison between the braking torque dynamic characteristics of FOESC and IOESC with (a) the ideal actuator and (b) the available bandwidth actuator.

braking torque has a 0.58s phase lag when searching for the optimal slip rate. The IOESC response time is 0.11 s, although 893 N·m torque overshoots still occur.

Fig. 6 (a) and Fig. 6 (b) compare the slip rate dynamic characteristics of FOESC and IOESC with the ideal actuator and the available bandwidth actuator, respectively, on the high adhesion road. Under the ideal conditions of the actuator, the slip rate of IOESC transitions quickly to the optimal slip rate of 0.11 in 0.27 s without overshoot. The slip rate of FOESC transitions quickly to the optimal slip rate of 0.11 in 0.03 s. The response speed of FOESC is better than IOESC. Corresponding to the braking torque, the slip rate also

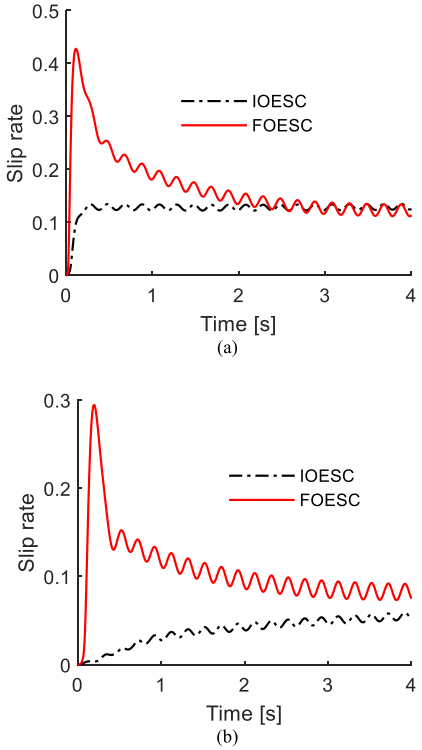

FIGURE 6. Slip rate curve on the high adhesion road. Comparison between the slip rate dynamic characteristics of FOESC and IOESC with (a) the ideal actuator and (b) the available bandwidth actuator.

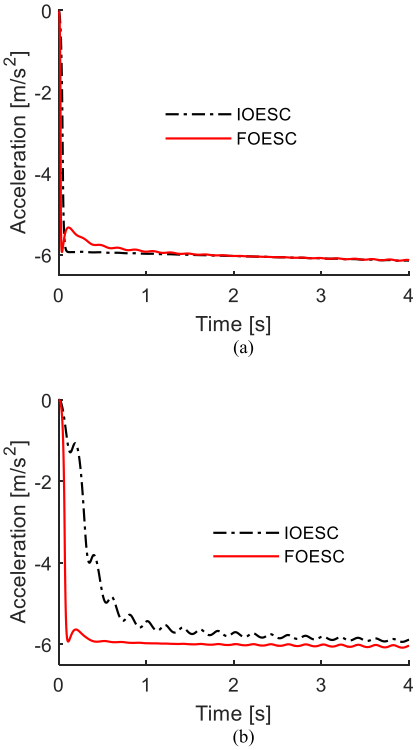

FIGURE 7. Braking deceleration on the high adhesion road. Comparison between the braking deceleration dynamic characteristics of FOESC and IOESC with (a) the ideal actuator and (b) the available bandwidth actuator.

produces overshoot with a peak value of 0.42. When the available bandwidth actuator is used, the convergence speed to the optimal slip rate of IOESC decreases. The slip rate overshoot peak of FOESC decreases to 0.28, but FOESC converges to the optimal slip rate in 0.4 s, which is faster than the convergence speed of IOESC.

Fig. 7 (a) and Fig. 7 (b) compare the braking deceleration dynamic characteristics of FOESC and IOESC with the ideal actuator and the available bandwidth actuator, respectively, on the high adhesion road. ESC brake deceleration quickly and smoothly transitions to the maximum braking speed in 0.10 s, which corresponds to the braking torque and slip rate. When the available bandwidth actuator is used, IOESC reaches the maximum braking deceleration in only 1.5 s, whereas FOESC converges to the maximum braking deceleration in 0.5 s. Moreover, the maximum braking deceleration obtained by FOESC, 6.04 m/s^2, is higher than that of IOESC, 5.71 m/s^2.

Comparing Fig. 5, Fig. 6 and Fig. 7 shows that the overshoot of the braking torque of FOESC makes the tire slip rate reach the optimal slip rate within a limited time. Because the vehicle needs to reach the optimal slip rate within a limited time, the actuator must provide the overshoot of the braking torque to get the optimal slip rate. If the tire slip rate remains optimal, the vehicle will attain the maximum braking deceleration. In a word, the overshoot of the braking torque creates the transient behavior of the vehicle, and the braking deceleration of the vehicle reaches the maximum rapidly. The braking deceleration of FOESC is greater than that of IOESC at the initial moment. The fractional theory analysis verifies that the fractional order improves the system lag caused by the integer order. Another reason is that the optimal slip rate estimated by FOESC has overshoot at the initial moment, which also leads to overshoot of the braking torque. Although the transient characteristics have overshoot, the braking deceleration obtained by FOESC is still better than that of IOESC. Of course, the increase in longitudinal acceleration inevitably leads to a decrease in ride comfort. However, for emergency braking, braking safety should be prioritized over ride comfort. Notably, the slip rate obtained by FOESC before 0.4 seconds is greater than the optimal value. This result leads to a slight decrease in the braking deceleration of the vehicle at the same time, which is consistent with the vehicle dynamics.

Fig. 8 (a) and Fig. 8 (b) compare the braking distance dynamic characteristics of FOESC and IOESC with the ideal actuator and the available bandwidth actuator, respectively, on the high adhesion road. Under the ideal actuator conditions, comparing the braking distance and vehicle speed of IOESC and FOESC shows that the braking distances of the two methods are almost 73.31 m. This result is determined by the nonlinear characteristics of the tire, and the friction torque provided by the ground near 0.1 and 0.4 fluctuates less. Thus, under the ideal conditions of brake actuators,

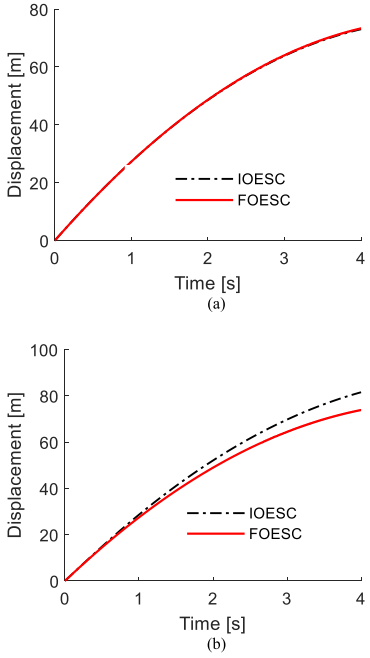

FIGURE 8. Braking distance on the high adhesion road. Comparison between the braking distance dynamic characteristics of FOESC and IOESC with (a) the ideal actuator and (b) the available bandwidth actuator.

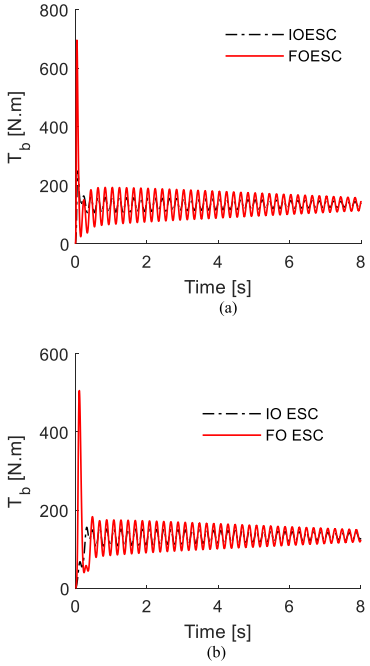

FIGURE 9. Braking torque on the low adhesion road. Comparison between the braking torque dynamic characteristics of FOESC and IOESC with (a) the ideal actuator and (b) the available bandwidth actuator.

on high-adhesion driving roads, both control methods achieve a good anti-lock braking performance. However, when the available bandwidth actuator is used, during the braking process from 30 m/s to 5 m/s, the braking distance of FOESC is 74.07 m and that of IOESC is 84.43 m, indicating that FOESC has better robustness than IOESC.

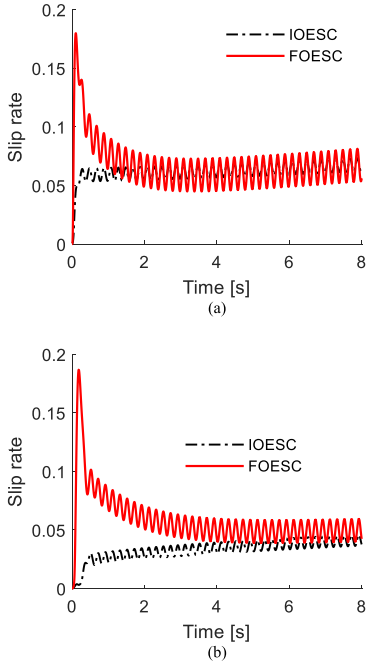

FIGURE 10. Slip rate on the low adhesion road. Comparison between the slip rate dynamic characteristics of FOESC and IOESC with (a) the ideal actuator and (b) the available bandwidth actuator.

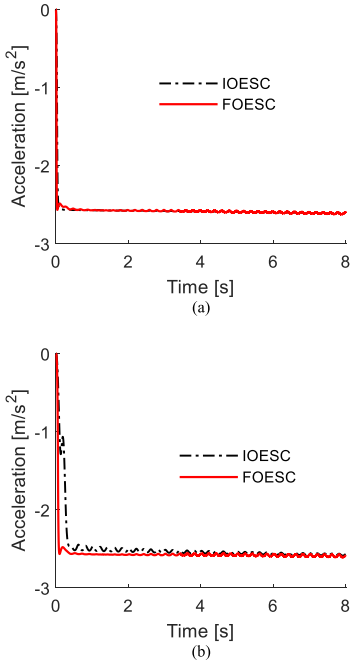

FIGURE 11. Braking deceleration on the low adhesion road. Comparison between the braking deceleration dynamic characteristics of FOESC and IOESC with (a) the ideal actuator and (b) the available bandwidth actuator.

Figs. 9-12 compare the braking performances of the two ABS control methods with the ideal actuator and the available bandwidth actuator on the low adhesion road. Consistent with the braking on the high adhesion road, both controllers

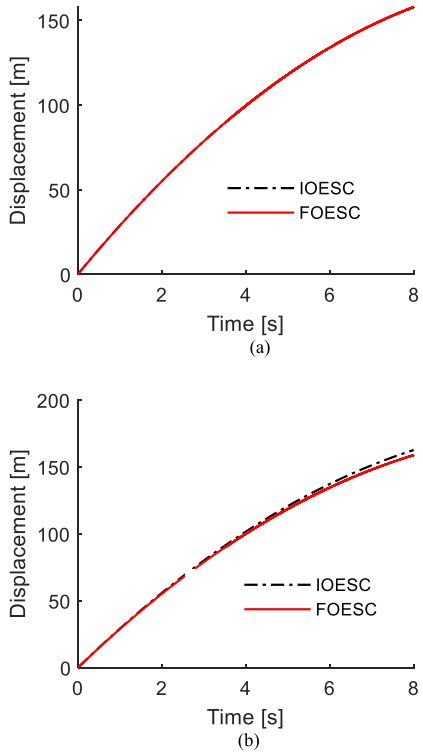

FIGURE 12. Braking distance on the low adhesion road. Comparison between the braking distance dynamic characteristics of FOESC and IOESC with (a) the ideal actuator and (b) the available bandwidth actuator.

achieve better braking effects without considering the actuator bandwidth. Neither the brake torque nor the slip rate amplitude of IOESC undergo overshoot. However, the braking torque of FOESC reaches 200 N·m in 0.06 s, and that of IOESC reaches 200 N·m in 0.42 s; FOESC has a faster braking torque response. When the actuator is limited by the bandwidth, compared with FOESC, the slip rate obtained by IOESC increases slowly and converges to the optimal slip rate of 0.68 in 4.2 s. The FOESC search slip rate converges to the optimal slip rate in 1.58 s. The braking deceleration controlled by FOESC reaches 2.57 m/s^2 in 0.06 s, and that controlled by IOESC reaches 2.49 m/s^2 in 0.42 s. The convergence speed of IOESC's search for the optimal slip rate and the response speed of reaching the maximum deceleration are low. During the braking process when the braking speed is reduced from 30 m/s to 5 m/s, the braking distance of the two controllers is approximately 158 m during the braking process with the ideal actuator, whereas the braking distance of FOESC is 158.8 m, while that of IOESC is 162.6 m, when the available bandwidth actuator is used.

To further analyze the control effect of the FOESC controller, simulations were performed on the road surface where the adhesion coefficient increased from 0.3 to 0.8, as shown in Fig. 13.

Fig. 14 (a) and Fig. 14 (b) compare the braking torque dynamic characteristics of FOESC and IOESC with the ideal

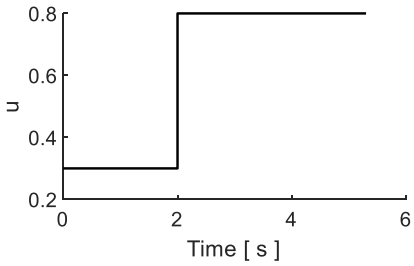

FIGURE 13. Adhesion coefficient curve with time.

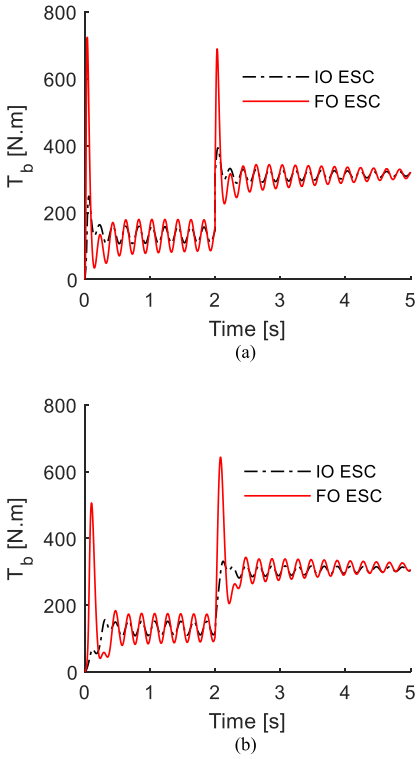

FIGURE 14. Tire braking torque on the changing road. Comparison between the braking torque dynamic characteristics of FOESC and IOESC with (a) the ideal actuator and (b) the available bandwidth actuator.

actuator and the available bandwidth actuator, respectively, on the changing road. Fig. 14 shows that when the actuator is not limited by the bandwidth, the braking torques of the two types of controls basically match. Only in the initial braking phase and on the road step changes does the FOESC braking torque have a peak torque, 720 N.m. When the actuator is limited by the bandwidth, the braking torque of IOESC has a 0.42 s hysteresis at the initial moment of braking, and the braking torque of IOESC has a 0.11 s hysteresis. The braking torque response speed of FOESC has also not been greatly affected.

Fig. 15 (a) and Fig. 15 (b) compare the slip rate dynamic characteristics of FOESC and IOESC with the ideal actuator and the available bandwidth actuator, respectively, on the changing road. When the actuator is not limited by the bandwidth, IOESC quickly transitions to the optimal slip rate

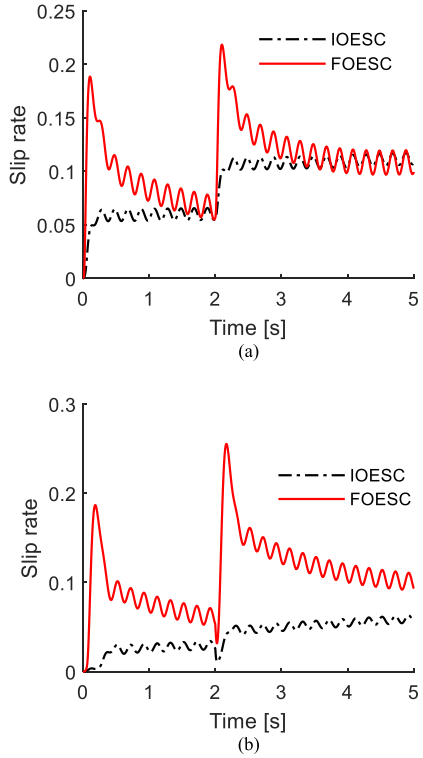

FIGURE 15. Slip rate on the changing road. Comparison between the slip rate dynamic characteristics of FOESC and IOESC with (a) the ideal actuator and (b) the available bandwidth actuator.

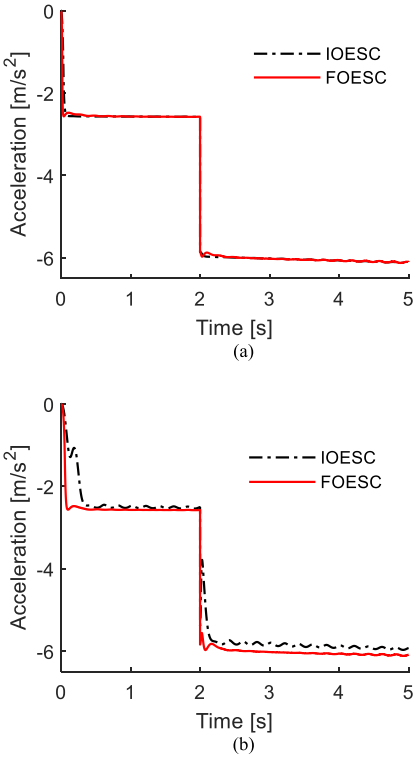

FIGURE 16. Braking deceleration on the changing road. Comparison between the braking deceleration dynamic characteristics of FOESC and IOESC with (a) the ideal actuator and (b) the available bandwidth actuator.

near 0.668 without overshoot. At 2 s, IOESC searched again quickly and without overshoot to obtain an optimal slip rate of 0.111. The slip rate controlled by FOESC produces a certain overshoot at the beginning of braking and at 2 s; when the available bandwidth actuator is used, the slip rates obtained by IOESC on the changing road are 0.03 and 0.06, respectively, which are not the optimal slip rate. FOESC searched for slip rates of 0.068 and 0.11 at 0.82 s and 3.2 s, respectively, on the changing road. The convergence speed of FOESC's search for an optimal slip rate is barely affected.

Fig. 16 (a) and Fig. 16 (b) compare the braking deceleration dynamic characteristics of FOESC and IOESC with the ideal actuator and the available bandwidth actuator, respectively, on the changing road. The acceleration controlled by the two controllers approximately transitioned from 2.6 m/s^2 to 6.0 m/s^2 under the condition that the actuator is not limited by the bandwidth. However, when the available bandwidth actuator is used, FOESC and IOESC attain the maximum braking deceleration of 2.5 m/s^2 in 0.1 s and 2.4 m/s^2 in 0.5 s, respectively. When the road changes in 2 s, FOESC and IOESC attain the maximum braking deceleration of 6.0 m/s^2 in 2.08 s and 5.8 m/s^2 in 2.20 s, respectively. Compared with FOESC, the IOESC process generates maximum braking deceleration slowly and to a smaller extent when the available bandwidth actuator is used.

Fig. 17 (a) and Fig. 17 (b) compare the braking distance dynamic characteristics of FOESC and IOESC with the ideal actuator and the available bandwidth actuator, respectively, on the changing road. During the braking process, when the braking speed is reduced from 30 m/s to 5 m/s, the braking distance of the two controllers is approximately 104.5 m under the condition that the actuator is not limited by the bandwidth. However, the braking distance of FOESC is 105.1 m and that of IOESC is 108.5 m when the available bandwidth actuator is used.

To demonstrate the advanced performance of FOESC, its braking distance is comprehensively compared to that of IOESC during the braking process when the vehicle speed is reduced from 30 m/s to 5 m/s, as shown in Table 2. Superscripts 1 and 2 indicates an ideal actuator without and with the bandwidth limitations, respectively.

Table 2 shows that, without considering the actuator bandwidth, the braking distance of FOESC in the ABS operation is almost identical to that of IOESC. Compared to IOESC, the largest performance reduction of FOESC is on the high adhesion road surface and is only 0.43%. However, after considering the actuator bandwidth, the braking distance of FOESC has been greatly improved compared to that of IOESC. When the ABS emergency braking is used on high-adhesion roads and low-adhesion roads, the braking distance of FOESC is 11% and 2.3% shorter than that of IOESC, respectively. Furthermore, the braking distance of FOESC was decreased by 3.1% compared with that of IOESC when the ABS braking was performed on the road step condition.

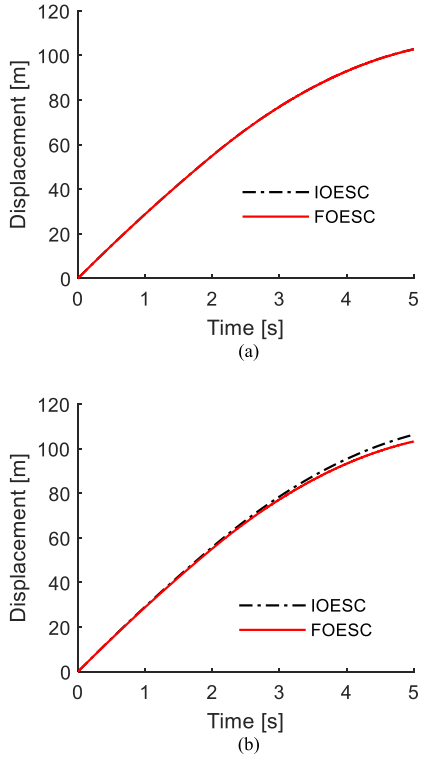

FIGURE 17. Braking distance on the changing road. Comparison between the braking distance dynamic characteristics of FOESC and IOESC with (a) the ideal actuator and (b) the available bandwidth actuator.

TABLE 2. Emergency braking distance.

Braking conditions	FOESC /m	IOESC /m
high adhesion [1]	74.39	74.07
medium adhesion [1]	108.8	108.7
low adhesion[1]	158	158.1
high adhesion [2]	75.17	84.43
medium adhesion [2]	110	116.6
low adhesion[2]	158.8	162.6
changing adhesion[1]	104.5	104.5
changing adhesion[2]	105.1	108.5

To investigate the effectiveness of FOESC, a comparison between the robust predictive control (RPC) and the FOESC is made regarding the changing road. The objective of the RPC is to track the wheel slip constant, which is 0.15.

Fig. 18 shows the braking torque dynamic characteristics of FOESC and RPC. Figure 18 shows that, at the initial moment, the peak braking torque of FOESC is 508 N·m, whereas that of RPC is 331 N·m. When the road changes, the peak braking torque of FOESC is 637 N·m, whereas that of RPC of 366 N·m. More importantly, the peak braking torque time of FOESC is 0.10 s and 2.08 s, while that of RPC is 0.12 s and 2.2 s, respectively. The braking torque of RPC is relatively gentle, while that of FOESC always has a sinusoidal periodic disturbance. This is because the nature of FOESC is caused by the nature of searching for the optimal value through a sinusoidal disturbance.

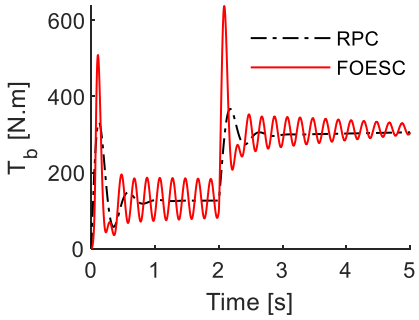

FIGURE 18. Comparison between the braking torque dynamic characteristics of RPC and FOESC with the available bandwidth actuator.

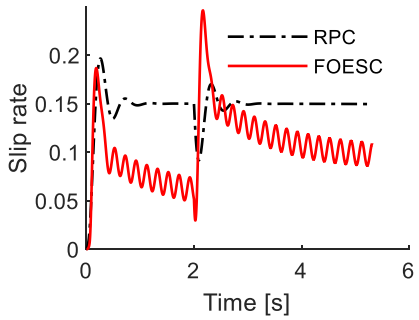

FIGURE 19. Comparison between the slip rate dynamic characteristics of FOESC and RPC with the available bandwidth actuator.

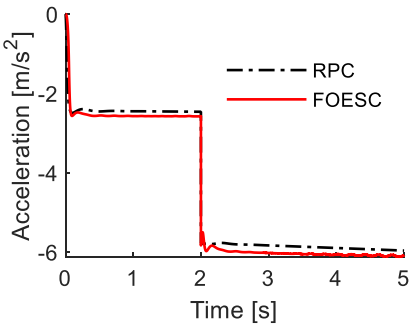

FIGURE 20. Comparison between the braking deceleration dynamic characteristics of FOESC and RPC with the available bandwidth actuator.

Fig. 19 shows that, at the initial moment of braking, the wheel slip rate is controlled by the RPC method and the FOESC method to 0.15 and 0.068, respectively. When the friction coefficient of the road changes, the wheel slip rate remains controlled by the RPC method at 0.15, while that controlled by the FOESC method is 0.11. This result shows that FOESC can obtain the optimal wheel slip rate according to different road surfaces, while the target wheel slip rate of RPC is not the optimal value.

Fig. 20 shows that, at the initial moment of braking, the braking deceleration controlled by the RPC method and the FOESC method is 2.45 m/s^2 and 2.57 m/s^2, respectively. At 2 s, the road friction coefficient changes, and the

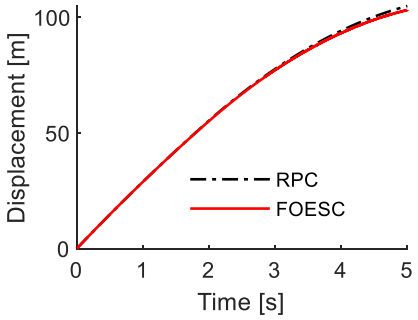

FIGURE 21. Comparison between the braking distance dynamic characteristics of FOESC and RPC with the available bandwidth actuator.

braking deceleration controlled by the RPC method and FOESC method is 5.86 m/s^2 and 6.04 m/s^2, respectively. This result shows that FOESC can obtain greater braking deceleration than RPC on different roads.

Fig. 21 shows that the braking distance of the car controlled by the FOESC method and the RPC method is 105.1 m and 106.6 m, respectively. FOESC decreases the braking distance of the car by 1.41% compared with that of the RPC method. This result shows that FOESC further improves the braking performance compared with the RPC method.

In terms of the computational effort and the possibility for implementation in a production of the ABS ECU, FOESC is an enhancement of ESC by fractional order operators. The fractional operator only needs to design an integer order continuous filter to fit the filter of the fractional action. These technologies are existing and mature, and the computational effort is not large. Introducing FOESC into the ECU of the ABS is technically possible. Furthermore, FOESC further improves the braking performance.

VI. CONCLUSION

In this research, an improved NPC enhanced by FOESC is proposed for the ABS considering the available actuator bandwidth. The key idea of the proposed controller is to use FOESC to improve the optimal slip rate search speed, which is limited by the bandwidth of the actuator. At the same time, the NPC is developed to predict the slip rate from the nonlinear vehicle model and control the optimal slip rate. The simulation results show that the IOESC and FOESC can search for the optimal slip rate regardless of the limitations of the actuator bandwidth. IOSEC is limited by the bandwidth of the actuator, and the convergence rate of the optimal slip rate becomes slower. FOESC is not greatly affected by the bandwidth of the actuator and can still quickly search for the slip rate. Compared with the traditional IOESC, the integrated controller of FOESC effectively obtains the optimal slip rate and implements effective tracking control under consideration of the actuator bandwidth. On the high adhesion road, the braking distance performance of FOESC is decreased by 11% compared with that of IOESC. In future works, it will be interesting to implement and analyze the proposed method on an actual vehicle considering the actuator time delay and the uncertainty of the test vehicle.

REFERENCES

[1] W. Zhao, Y. Wang, and C. Wang, "Multidisciplinary optimization of electric-wheel vehicle integrated chassis system based on steady endurance performance," *J. Cleaner Prod.*, vol. 186, pp. 640–651, Jun. 2018.

[2] F. Pretagostini, L. Ferranti, G. Berardo, V. Ivanov, and B. Shyrokau, "Survey on wheel slip control design strategies, evaluation and application to antilock braking systems," *IEEE Access*, vol. 8, pp. 10951–10970, 2020.

[3] R. He and Z. C. Jing, "Study on braking stability of commercial vehicles: An optimized air brake system," *Adv. Mech. Eng.*, vol. 11, no. 5, p. 10, May 2019.

[4] J. Wang and R. He, "Varying charge voltage in the steps control method of ABS for in-wheel motors driven electric vehicles based on an improved LQG scheme," *IEEE Access*, vol. 6, pp. 15039–15050, 2018.

[5] A. Mousavi, A. H. Davaie-Markazi, and S. Masoudi, "Comparison of adaptive fuzzy sliding-mode pulse width modulation control with common model-based nonlinear controllers for slip control in antilock braking systems," *J. Dyn. Syst., Meas., Control*, vol. 140, no. 1, p. 15, Jan. 2018.

[6] X. Zhao, L. Li, J. Song, C. Li, and X. Gao, "Linear control of switching valve in vehicle hydraulic control unit based on sensorless solenoid position estimation," *IEEE Trans. Ind. Electron.*, vol. 63, no. 7, pp. 4073–4085, Jul. 2016.

[7] C. Lv, H. Wang, and D. Cao, "High-precision hydraulic pressure control based on linear pressure-drop modulation in valve critical equilibrium state," *IEEE Trans. Ind. Electron.*, vol. 64, no. 10, pp. 7984–7993, Oct. 2017.

[8] S. Rajendran, S. Spurgeon, G. Tsampardoukas, and R. Hampson, "Time-varying sliding mode control for ABS control of an electric car," *IFAC-Papers Line*, vol. 50, no. 1, pp. 8490–8495, Jul. 2017.

[9] S. Chen and X. L. J. Z. Zhang andWang, "Sliding Mode Control of Vehicle Equipped with Brake-by-Wire System considering Braking Comfort," *Shock Vib.*, vol. 2020, p. 13, Feb. 2020.

[10] Y. Tang, Y. Wang, M. Han, and Q. Lian, "Adaptive fuzzy fractional-order sliding mode controller design for antilock braking systems," *J. Dyn. Syst., Meas., Control*, vol. 138, no. 4, Apr. 2016.

[11] H. Mirzaeinejad and M. Mirzaei, "A novel method for non-linear control of wheel slip in anti-lock braking systems," *Control Eng. Pract.*, vol. 18, no. 8, pp. 918–926, Aug. 2010.

[12] H. Mirzaeinejad, "Robust predictive control of wheel slip in antilock braking systems based on radial basis function neural network," *Appl. Soft Comput.*, vol. 70, pp. 318–329, Sep. 2018.

[13] R. E. Precup, "Evolving fuzzy models for anti lock braking systems," in *Proc. CIVEMSA*, Annecy, France, 2017, pp. 48–53.

[14] C.-M. Lin and T.-L. Le, "PSO-Self-Organizing interval Type-2 fuzzy neural network for antilock braking systems," *Int. J. Fuzzy Syst.*, vol. 19, no. 5, pp. 1362–1374, Oct. 2017.

[15] B. Chen, "Simulation analysis of automobile ABS based on artificial neural network," in *Proc. 2nd Int. Conf. Mater. Sci., Machinery Energy Eng. (MSMEE)*, 2017, pp. 1812–1817.

[16] M.-B. Radac and R.-E. Precup, "Data-driven model-free slip control of anti-lock braking systems using reinforcement Q-learning," *Neurocomputing*, vol. 275, pp. 317–329, Jan. 2018.

[17] A. Digrase and A. Wayse, "Model following control for anti-lock braking system with inertial delay observer," in *Proc. Int. Conf. Intell. Comput. Control Syst. (ICICCS)*, Jun. 2017, pp. 467–471.

[18] Y. Tang, X. Zhang, D. Zhang, G. Zhao, and X. Guan, "Fractional order sliding mode controller design for antilock braking systems," *Neurocomputing*, vol. 111, pp. 122–130, Jul. 2013.

[19] Y. He, C. Lu, J. Shen, and C. Yuan, "Design and analysis of output feedback constraint control for antilock braking system based on Burckhardt's model," *Assem. Autom.*, vol. 39, no. 4, pp. 497–513, Sep. 2019.

[20] W. L. Yong, "Research on the real-time identification approach of longitudinal road slope and maximum road friction coefficient," *Int. J. Veh. Des.*, vol. 79, no. 1, pp. 18–42, 2019.

[21] Y. Shiozawa and H. Mouri, "Proposal of the road surface friction coefficient real-time estimation method," *J. Adv. Mech. Des. Syst. Manuf.*, vol. 12, no. 7, p. 12, 2018.

[22] Y.-Q. Zhao, H.-Q. Li, F. Lin, J. Wang, and X.-W. Ji, "Estimation of road friction coefficient in different road conditions based on vehicle braking dynamics," *Chin. J. Mech. Eng.*, vol. 30, no. 4, pp. 982–990, Jul. 2017.
[23] K. B. Ariyur, and M. Krstic, *Real-Time Optimization by Extremum-Seeking Control*. Hoboken, NJ, USA: Wiley, 2003, pp. 1–19.
[24] C. Zhang, and R. Ordóñez, *Extremum-Seeking Control and Applications: A Numerical Optimization-Based Approach*. New York, NY, USA: Springer, 2011.
[25] H. Malek and Y. Chen, "Fractional order extremum seeking control: Performance and stability analysis," *IEEE/ASME Trans. Mechatronics*, vol. 21, no. 3, pp. 1620–1628, Jun. 2016.
[26] H. Yu and U. Ozguner, "Extremum-seeking control strategy for ABS system with time delay," in *Proc. Amer. Control Conf.*, 2002, pp. 3753–3758.
[27] C. Zhang and R. Ordonez, "Numerical optimization-based extremum seeking control with application to ABS design," *IEEE Trans. Autom. Control*, vol. 52, no. 3, pp. 454–467, Mar. 2007.
[28] E. Dincmen, B. A. Guvenc, and T. Acarman, "Extremum-seeking control of ABS braking in road vehicles with lateral force improvement," *IEEE Trans. Control Syst. Technol.*, vol. 22, no. 1, pp. 230–237, Jan. 2014.
[29] G. Stein, "Respect the unstable," *IEEE Control Syst.*, vol. 23, no. 4, pp. 12–25, Aug. 2003.
[30] A. Oustaloup, F. Levron, B. Mathieu, and F. M. Nanot, "Frequency-band complex noninteger differentiator: Characterization and synthesis," *IEEE Trans. Circuits Syst. I, Fundam. Theory Appl.*, vol. 47, no. 1, pp. 25–39, Jan. 2000.
[31] A. Harifi, A. Aghagolzadeh, G. Alizadeh, and M. Sadeghi, "Designing a sliding mode controller for slip control of antilock brake systems," *Transp. Res. C, Emerg. Technol.*, vol. 16, no. 6, pp. 731–741, Dec. 2008.
[32] C. Satzger and R. de Castro, "Predictive brake control for electric vehicles," *IEEE Trans. Veh. Technol.*, vol. 67, no. 2, pp. 977–990, Feb. 2018.

REN HE was born in Nanjing, Jiangsu, China, in 1962. He received the B.S. degree from Jiangsu University, Zhenjiang, China, in 1983, the M.S. degree from Jilin University, Changchun, in 1986, and the Ph.D. degree from Jiangsu University, in 1995.

He has been a Professor with Jiangsu University, since 1997, where he is also the Director of Automotive Engineering Key Laboratory of Jiangsu Province. He has authored or coauthored more than 100 published refereed technical articles and five books. He also holds more than 100 patents. His research interests include integrated automotive energy conservation, hybrid powertrain theory and method of regenerative braking of automobile, integrated control, and optimization of powertrain. He received the Special Allowance of the State Council of China.

LEI YUAN was born in Rizhao, Shandong, China, in 1991. He received the B.S. degree from the Shandong University of Technology, Zibo, China, in 2013, and the M.S. degree from Jiangsu University, Zhenjiang, China, in 2018, where he is currently pursuing the Ph.D. degree.

His research interests include vehicle system dynamics and electric vehicle technology.